ACS EARTH AND SPACE CHEMISTRY

Article

Reactive Uptake of Isoprene Epoxydiols Increases the Viscosity of the Core of Phase-Separated Aerosol Particles

Nicole Olson, Ziying Lei, Rebecca Lynn Craig, Yue Zhang, Yuzhi Chen, Andrew T. Lambe, Zhenfa Zhang, Avram Gold, Jason Douglas Surratt, and Andrew P Ault

ACS Earth Space Chem., **Just Accepted Manuscript** • DOI: 10.1021/acsearthspacechem.9b00138 • Publication Date (Web): 21 Jun 2019

Reactive Uptake of Isoprene Epoxydiols Increases the Viscosity of the Core of Phase-Separated Aerosol Particles

Nicole E. Olson[1], Ziying Lei[2], Rebecca L. Craig[1†], Yue Zhang[3, 4], Yuzhi Chen[3], Andrew T. Lambe[4], Zhenfa Zhang[3], Avram Gold[3], Jason D. Surratt[3*], Andrew P. Ault[1, 2*]

[1]Department of Chemistry, University of Michigan, Ann Arbor, Michigan, 48109

[2]Department of Environmental Health Sciences, University of Michigan, Ann Arbor, Michigan, 48109

[3]Department of Environmental Sciences and Engineering, Gillings School of Global Public Health, University of North Carolina at Chapel Hill, Chapel Hill, North Carolina, United States 27599

[4]Aerodyne Research Inc., Billerica, Massachusetts, United States 01821

[†]Current affiliation: Department of Chemistry, The College of Wooster, Wooster, Ohio, 44691

*corresponding authors: Andrew Ault: aulta@umich.edu
Jason Surratt: surratt@unc.edu

Keywords: Aerosol Phase State, Aerosol Viscosity, Isoprene Epoxydiol (IEPOX), Microscopy, Secondary Organic Aerosol (SOA)

Abstract (250 words)

Atmospheric oxidation of volatile organic compounds, such as isoprene, and subsequent condensation or heterogeneous reactions lead to the formation of secondary organic aerosol (SOA), a ubiquitous component of submicron aerosol. Liquid-liquid phase-separated organic-inorganic aerosol particles have been observed in the laboratory and field; however, the impacts of multiphase reactions on aerosol viscosity are not well understood for phase-separated aerosol particles. In this study, phase-separated aerosol particles were reacted with gaseous isoprene epoxydiol (IEPOX), an abundant isoprene oxidation product. Acidic sulfate particles (H_2SO_4 + $(NH_4)_2SO_4$ at pH = 1.4) were coated with laboratory-generated biogenic SOA (α-pinene + O_3) and anthropogenic SOA (toluene + OH), resulting in a core-shell morphology. After reaction with IEPOX, the phase-separated aerosol particles no longer displayed characteristics of a liquid core. Instead, they became irregularly shaped, taller after impaction onto substrates, and had decreased spreading ratios for both types of SOA, implying an increase in particle viscosity. As the SOA from α-pinene and toluene was already viscous, this is indicative of a change in phase state for the core from liquid to viscous state. An example reaction that may be facilitating this phase change is IEPOX reaction with inorganic sulfate to produce organosulfates, especially after IEPOX diffuses through the organic coating. The modification of the aerosol physicochemical properties suggests that phase state is dynamic over the atmospheric lifetime of SOA-containing particles, with multiphase chemistry between aerosol particles and gaseous species leading to more viscous aerosol after uptake of isoprene oxidation products (e.g. IEPOX).

Introduction

Climate-relevant aerosol properties, such as the ability to scatter or absorb solar radiation and alter cloud or precipitation patterns by acting as cloud condensation nuclei (CCN) and ice nuclei (IN),[1-3] are dependent on individual particle physiochemical properties, including chemical composition, aerosol phase, and morphology.[1,2,4,5] These properties are dynamic as the diurnal cycle of relative humidity (RH) modifies the water content of aerosols and, thus, alters the physical state of particles, including particle phase state and viscosity.[6-9] Changes in RH and particle composition can both lead to transitions of particle phase states,[7-12] which range from liquid and semi-solid to glassy and crystalline state, and can include the separation of phases within individual aerosol particles.[13,14] Phase-separated particles typically form when inorganic and organic phases are no longer miscible at higher molar concentrations at lower RH.[11] Inorganic particles, particularly sulfate-containing particles, can react with gas-phase organic species generated by gas-phase oxidation of biogenic and anthropogenic volatile organic compounds (VOCs).[1,11,15,16] For instance, isoprene and α-pinene are major VOCs emitted from vegetation,[17,18] while toluene is a ubiquitous anthropogenic VOC.[19] Oxidation products of VOCs condensing onto existing inorganic aerosols leads to the formation of secondary organic aerosol (SOA), accounting for more than 50% of the total organic aerosol mass globally.[20,21]

Isoprene, the most abundant non-methane hydrocarbon emitted into the atmosphere (~600 Tg y^{-1}),[17,22] undergoes oxidation by hydroxyl radicals to form large quantities of gaseous isoprene epoxydiols (IEPOX) under low-NO_x conditions.[23,24] The increased molecular functionality and associated decrease in vapor pressure that occurs from the oxidation of isoprene (0.62 atm at 293 K) to IEPOX (3.4×10^{-6} atm at 293 K) facilitates uptake into the particle phase via multi-phase chemical reactions,[16,20,25-27] particularly under acidic conditions.[28,29] IEPOX-derived SOA has

been shown to contribute up to 40% of submicron organic aerosol mass in isoprene-rich environments,[30,31] contributing to changes in aerosol physiochemical properties.[13,32] However, to date, few studies have analyzed changes in SOA physiochemical properties (particle morphology, viscosity, and phase) after IEPOX uptake. Individual particle measurements are necessary to provide better understanding of the effect of IEPOX uptake on particle morphology and phase, which impact how particles participate in light scattering and climate-altering processes.[33,34]

Phase separation within atmospheric aerosol particles has a wide range of atmospheric implications, including altering SOA formation by modifying the partitioning of organic species from the gas to particle phase.[35-37] This includes either inhibition[7-12,32,36,38] or enhancement of reactive uptake to particles containing more than one phase[39] typically an organic outer layer and an aqueous-inorganic core.[40] Given that these results have primarily been based on thermodynamic models, further experimental data is needed on the uptake of key oxidation products for phase separated particles. Phase separations have also been shown to increase solar radiation scattering and absorption.[41] Therefore, determining aerosol phase, phase separations, and morphology (e.g. core-shell) is necessary to accurately predict atmospheric SOA formation and aerosol impacts on air quality and radiative forcing.

SOA species can exist in glassy, highly viscous states that alter aerosol reactivity.[18,42-44] Multiphase chemistry of IEPOX in the ambient environment leads to the formation of organosulfates,[45-48] polyols,[20,47,49,50] and oligomers[27,49,51,52] in the condensed phase, thereby increasing particle viscosity. Viscosity alters mixing timescales and diffusion throughout the particle, with potential to change the particle phase from homogeneously mixed to phase-separated.[53] Highly viscous organic phases can kinetically inhibit the transfer of mass and, thus, inhibit phase transitions and gas-particle partitioning.[18,42-44,54-56] More viscous particles have lower

gaseous uptake,[18,32] reactivity,[18,44] and limited particle growth,[18] impacting particle evolution in the atmosphere.[7] However, the relationship between reactive uptake, particle viscosity, and phase separation is not well characterized for mixed SOA-inorganic particles, the dominant particle type, by number, in the Southeastern United States.[15]

To date, laboratory studies investigating phase separation have primarily been conducted using inorganic particles coated with organic acids (pimelic,[10,57] succinic,[10,12,57] glutaric[9,12]), sucrose,[12] and decane.[58] Additional laboratory studies have investigated phase separation of more chemically complex, atmospherically-relevant biogenically-derived SOA, such as α-pinene SOA.[14,38,59] However, investigations of α-pinene SOA using imaging methods as direct evidence of phase separation[14,59] focused on 8.5 – 30 μm particles, a size range that is significantly larger than the number and mass modes of atmospheric particulate matter (PM),[2] and therefore might not be an accurate representation of particle phase at smaller sizes due to the size-dependent kinetic effects observed in Veghte et al.[57] Virtanen et al.[43] found laboratory-generated 100 nm α-pinene SOA particles exhibited semi-solid behavior based on particle bounce measurements. However, this study was performed at 30% RH, which is much lower than the 50-90% ambient RH reported by field studies in the Southeast United States where IEPOX-derived SOA is prevalent,[60] and therefore might influence the particle phase state observed.[14] Studies examining α-pinene SOA at higher RH found particles to have semi-solid behavior up to 90% RH,[61] but particle morphology (homogeneous versus phase-separated) was not investigated across the different RH conditions. Bertram et al.[62] and Ciobanu et al.[63] systematically studied phase separation as a function of RH for laboratory-generated SOA and inorganic sulfate mixtures using optical microscopy, though they used 20–30 μm particles that are much larger than atmospheric SOA particles. Additional studies have analyzed the phase separation of laboratory-generated SOA from 0–100% RH.[38,64]

However, most used SOA in the absence of seed particles so the results are not directly comparable to the phase states presented herein. Particle coatings in boreal forest regions, where α-pinene SOA is dominant,[65] can behave differently than particle coatings in regions where isoprene and α-pinene emissions are both abundant, as shown recently by Slade et al.[13] Additional insights into atmospherically relevant sizes of α-pinene and isoprene SOA infer phase separation based on indirect methods such as an aerosol mass spectrometer (AMS),[66] scanning mobility particle sizer (SMPS),[66,67]tandem differential mobility analyzer,[68,69] and single particle ablation time-of-flight mass spectrometer (SPLAT),[36,67] providing information on particle size and phase state at different RH. Smith et al. found lower efflorescence and deliquescence RHs of isoprene-derived SOA[68] and α-pinene SOA[69] coated onto sulfate particles compared to pure ammonium sulfate particles, indicating changes in aerosol hygroscopic phase transitions with addition of SOA material. You et al.[14] showed aerosols can undergo phase separation after extraction of bulk particle organic material from filters. While informative, bulk measurements are unable to determine the number and composition of individual phase-separated atmospheric particles, but rather show that in 30 μm particles that the bulk SOA phase separates from an aqueous, inorganic phase. Song et al.[70] measured the phase state of toluene-derived anthropogenic SOA, obtaining results demonstrating that pure toluene-derived SOA particles become more viscous at lower RH. While these studies made important contributions to understanding biogenic and anthropogenic organic aerosol phases, we lack characterization of the changes in particle phase state after the reactive uptake of additional gaseous species, particularly for mixed organic-inorganic systems. Microscopic studies that directly investigate aerosol phase using single particles of atmospherically relevant size, composition, and RH are necessary to determine the factors influencing phase separation in particles, and particle phase changes following reaction with gaseous species.

In this study, we analyzed changes in particle phase state and viscosity after uptake of gas-phase IEPOX onto phase-separated α-pinene and toluene SOA-coated inorganic particles. Particles were characterized using atomic force microscopy (AFM), scanning electron microscopy coupled with energy dispersive x-ray spectroscopy (SEM-EDX), and Raman microspectroscopy to study the particle phase, morphology, and composition before and after IEPOX reactive uptake. Phase separation was influenced by particle size, with most small SOA particles (< 100 nm) remaining homogeneous and particles > 100 nm showing distinct phase-separated core-shell morphology, as confirmed by microscopic images and compositional differences between particle core and shell. Significant changes to particle core phase and morphology were observed after IEPOX reactive uptake, suggesting IEPOX diffusion through the outer organic shell to react with the inorganic core and modification of its physiochemical properties. Overall particle viscosity increased after IEPOX uptake, as shown by measurements of particle heights and spreading ratios, likely driven by a more viscous core. These changes to phase and morphology have important implications for further multi-phase chemical reactions and SOA formation.

Materials and Methods

Aerosol Generation

The system for generating SOA-coated sulfate particles was previously described in detail in Zhang et al.[32] and shown in Figure S1. Briefly, acidic ammonium sulfate particles (pH = 1.4 ± 0.2) were generated by atomizing a solution of 0.06 M ammonium sulfate ($(NH_4)_2SO_4$, Sigma Aldrich, ≥99% purity) and 0.06 M sulfuric acid (H_2SO_4, Sigma Aldrich, ≥98% purity) using a constant output atomizer (TSI Inc., Model 3076) to simulate the pH of ambient aerosol particles in the southeastern United States.[60] Initial particle pH was confirmed using the pH indicator method described in Craig et al.[71] Aerosols passed through a diffusion drier to remove excess water

resulting in particle RH of 26 ±3%, remaining near the efflorescence point of 34% RH.[72] A differential mobility analyzer (DMA, TSI Inc., Model 3080) was used to size select seed particles with 100 nm electrical mobility diameter. The DMA operated at a 12:3 sheath:sample flow ratio over the mobility size range of 10 – 600 nm, resulting in a number size distribution with a mode at 100 nm and a geometric standard deviation of 1.5 for acidic seed particles.[32]

A Potential Aerosol Mass (PAM) oxidation flow reactor (OFR; Aerodyne Research Inc.)[73] was used to generate SOA coatings on sulfate seed particles via ozonolysis of 200 ppb α-pinene or photooxidation of 800 ppb toluene. The OFR was operated in continuous flow mode with a mean residence time of 2 min. To establish ozonolysis conditions, 40 ppm O_3 was added at the inlet of the OFR using an external O_3 chamber. To establish photooxidation conditions, the O_3 was photolyzed at λ of 254 nm inside the OFR to generate $O(^1D)$ radicals, which reacted with H_2O to continuously produce hydroxyl (OH) radicals ([OH] ~10^{10} cm^{-3}). Recent studies suggest that SOA particles generated in OFRs have compositions similar to SOA generated in environmental chambers[56,74-77] and in the atmosphere.[78-83]

The aerosol-laden flow exiting the OFR was passed through two Nafion tubes (Perma Pure, Model PD-200T-12) to control and vary the RH prior to performing IEPOX uptake in a glass flow tube (1 m length, 8 cm ID, 40 s residence time) coated with halocarbon wax (Halocarbon Products Corporation) to minimize wall loss. IEPOX uptake was conducted using authentic *trans*-β-IEPOX, which is the predominant IEPOX isomer in the atmosphere,[23] and was synthesized following published procedures.[84] At the inlet and outlet of the glass flow tube, aerosols were collected for microscopy and spectroscopy analysis (details below). Aerosol size distributions were measured by a SMPS consisting of a DMA and a condensation particle counter (CPC, TSI Inc., Model 3022A) at the end of the flow tube.

Microscopy and Spectroscopy Analysis

Aerosol particles were collected for microscopy and spectroscopy analysis before and after IEPOX reactive uptake using a 3-stage microanalysis particle sampler (MPS-3, California Measurements Inc.). Particles were impacted onto carbon-type-b Formvar coated copper transmission electron microscopy (TEM) grids (Ted Pella Inc.), silicon wafers (Ted Pella Inc.), and quartz slides (Ted Pella Inc.) for SEM, AFM, and Raman analysis, respectively. Samples from stage 3 (aerodynamic diameter (d_a) < 400 nm) were selected for analysis. Particle morphology was classified as homogeneous or phase-separated based on the criteria defined in Veghte et al,[57] where non-phase-separated particles were visually homogeneous and phase-separated particles contained two or more immiscible substances. AFM and Raman measurements were performed at ambient pressure and RH (30-40%), while SEM was performed under vacuum conditions (10^{-5}-10^{-6} Torr). Because the ambient RH at which particles were imaged using AFM (30-40% RH) was lower than RH when samples were generated (50% RH), samples were re-humidified to 50% RH and imaged with AFM to investigate possible morphology changes resulting from humidity changes to the sample. As shown in Figure S2, re-humidified samples did not show significant differences in morphology compared to samples imaged at ambient RH. Therefore, AFM images and data in this text were collected at the ambient RH values of 30-40%.

SEM analysis was performed on an FEI Helios 650 Nanolab Dualbeam electron microscope that operated at an accelerating voltage of 10.0 kV and a current of 0.40 nA. The Helios microscope was equipped with a high angle annular dark field (HAADF) detector that provided contrast between areas of different elemental composition.[85] EDX spectra were acquired for 20 seconds using an EDAX detector and GENESIS EDX software version 5.10 (EDAX Inc., Mahwah, NJ). To investigate trends between particle size and phase separation, SEM images were

analyzed with image processing software (ImageJ, version 1.50i, National Institutes of Health, USA) to determine individual particle projected area diameters (diameter of particles after impaction onto substrate). Projected area diameters were then converted to volume equivalent diameters (d_{ve}) to simulate particle diameter before impaction and spreading onto substrate.[86] Volume equivalent diameters were calculated using particle volume data obtained from AFM analysis (described below) and the following equation, assuming particles were initially spheres before impaction:[86]

$$\text{Volume Equivalent Diameter } (d_{ve}) = \sqrt[3]{\frac{6 * \text{Particle Volume}}{\pi}} \qquad \text{Eq. (1)}$$

AFM was performed with a PicoPlus 5500 AFM (Agilent, Santa Clara, CA) that operated using 300 kHz resonant frequency and 40 N/m spring constant. Tapping mode was performed utilizing Aspire CT300R probes (NanoScience, AZ) to obtain phase and height images. Samples were scanned in 5 μm x 5μm areas with 0.75 Hz scan rates to obtain 512 pixels per line. Raw data was processed using SPIP 6.2.6 software (Image Metrology, Hørsholm, Denmark) to measure particle height, radius, and d_{ve}. Spreading ratios of individual particles were then calculated using the following equation:[87]

$$\text{Spreading Ratio} = \frac{\text{Particle radius (r)}}{\text{Particle height (h)}} \qquad \text{Eq. (2)}$$

T-tests were performed by comparing the mean spreading ratio of each sample to the mean spreading ratio of the sulfate seed aerosol. SOA-coated particles exposed to IEPOX were also statistically analyzed with respect to SOA-coated particles. Spreading ratios were considered to be statistically different for p values < 0.05.

Raman microspectroscopy was conducted using a Horiba LabRAM HR Evolution Raman Spectrometer (Horiba Scientific) equipped with a 50mW 532 nm Nd:YAG laser source, CCD detector and coupled to a confocal optical microscope (Olympus, 100x objective). Raman spectra

were collected in the range 500-4000 cm^{-1} for 3 accumulations at 10 second acquisition times for each particle. A diffraction grating of 600 grove/mm with spectral resolution of 1.7 cm^{-1} was used.

Results and Discussion

Single particles were analyzed for phase and composition at three experimental points: 1) initial acidic ammonium sulfate seed particles with no SOA coating, 2) seed particles coated with α-pinene or toluene SOA, and 3) seed particles coated with SOA and exposed to IEPOX. Figure 1 is a schematic representing the changes in particle phase and morphology of single particles obtained at each step in the experiment. Acidic seed particles were expected to be homogeneous, characterized by a single aqueous phase with spherical morphology. Following the coating stage of each experiment by either α-pinene or toluene SOA, the particles are expected to experience phase separation resulting in a core-shell morphology consisting of a viscous organic coating and aqueous inorganic core. Modeling the properties of the α-pinene or toluene SOA organic layers predicts viscosities of 10^3-10^9 Pa s for α-pinene SOA[7,88] and 10^2-10^7 Pa s for toluene SOA at 50% RH based on O:C measurements from an aerosol chemical speciation monitor (ACSM).[70,88] This range of viscosities corresponds to semi-solid material[89,90] with mixing times of 2.8 h for α-pinene coated SOA and < 1 h for toluene coated SOA at 50% RH for particles < 1 μm diameter.[70] Uptake of IEPOX vapor is expected to induce particle phase processing that changes the phase state of the inorganic core from aqueous to semi-solid following the diffusion of IEPOX through the SOA coating.[32] The SOA coating inhibited some uptake into the particle, in comparison to an uncoated acidic aqueous particle.[32] Predicted IEPOX diffusion times through the organic coating ranged from 10^1-10^4 seconds with a reduction in the reactive uptake coefficient (γ) of ~50% for α-pinene SOA compared to an uncoated acidic particle.[32] Though IEPOX uptake was reduced, uptake was sufficient for significant acid-catalyzed particle-phase chemistry to occur. The continuing

chemistry changed the core of the particles from aqueous to a viscous or semi-solid core. The phase transitions of the particle core are shown below using a combination of AFM, SEM-EDX, and Raman microspectroscopy.

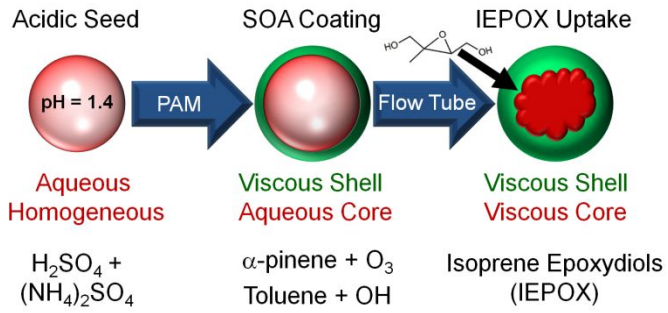

Figure 1. Schematic of experimental design showing anticipated particle phase state at each step. First, homogeneous seed particles were generated with an atomizer using solutions of ammonium sulfate and sulfuric acid to achieve an initial pH of 1.4. Next, seed particles were coated with α-pinene or toluene SOA in a Potential Aerosol Mass (PAM) reactor to achieve a coating thickness of ~10 nm before impaction onto substrates and spreading. SOA-coated seed particles were then exposed to gaseous isoprene epoxydiol (IEPOX) in a flow tube.

To demonstrate the changes in particle phase after coating and IEPOX uptake, AFM and SEM images of the three particle types are shown in Figure 2. Acidic ammonium sulfate seed particles were homogeneous in phase and composition with a circular morphology, indicative of a spherical shape when suspended, before addition of SOA coatings **(Figure 2a)**. The circular morphology indicates the particles were still liquid and above the efflorescence point,[72] per the experimental design.[32] After coating with SOA, the mixed sulfate-SOA particles exhibited core-shell morphology[57] with a circular sulfate core and SOA shell **(Figure 2b and 2d)**. These coated SOA particles were similar to ambient particles observed during the Southern Oxidant and Aerosol Study (SOAS) in the Southeastern United States during a period of high SOA production (Figure S3).[15] Following IEPOX uptake, particles still exhibited phase separation, but changes to the core morphology were observed for both α-pinene SOA/sulfate particles and toluene SOA/sulfate particles **(Figure 2c and 2e)**. Particle cores became non-circular with a variety of irregular shapes.

The less viscous organic coating filled in along the irregular surface created by the viscous core to leave the overall particle morphology spherical, consistent with the outer spherical morphology observed before IEPOX uptake. These core morphology changes suggest IEPOX diffused through the organic shell and reacted with the inorganic core to form viscous IEPOX-derived organosulfates.[45-48] AFM showed phase separation after SOA coating and core morphology changes after IEPOX uptake at ambient temperature and RH. SEM corroborated the phase and morphology observed by AFM. The images in Figure 2 show α-pinene and toluene SOA-coated inorganic sulfate particles generated at 50% RH. Additional samples generated at 30% RH show similar trends with respect to phase and morphology (Figures S4 and S5).

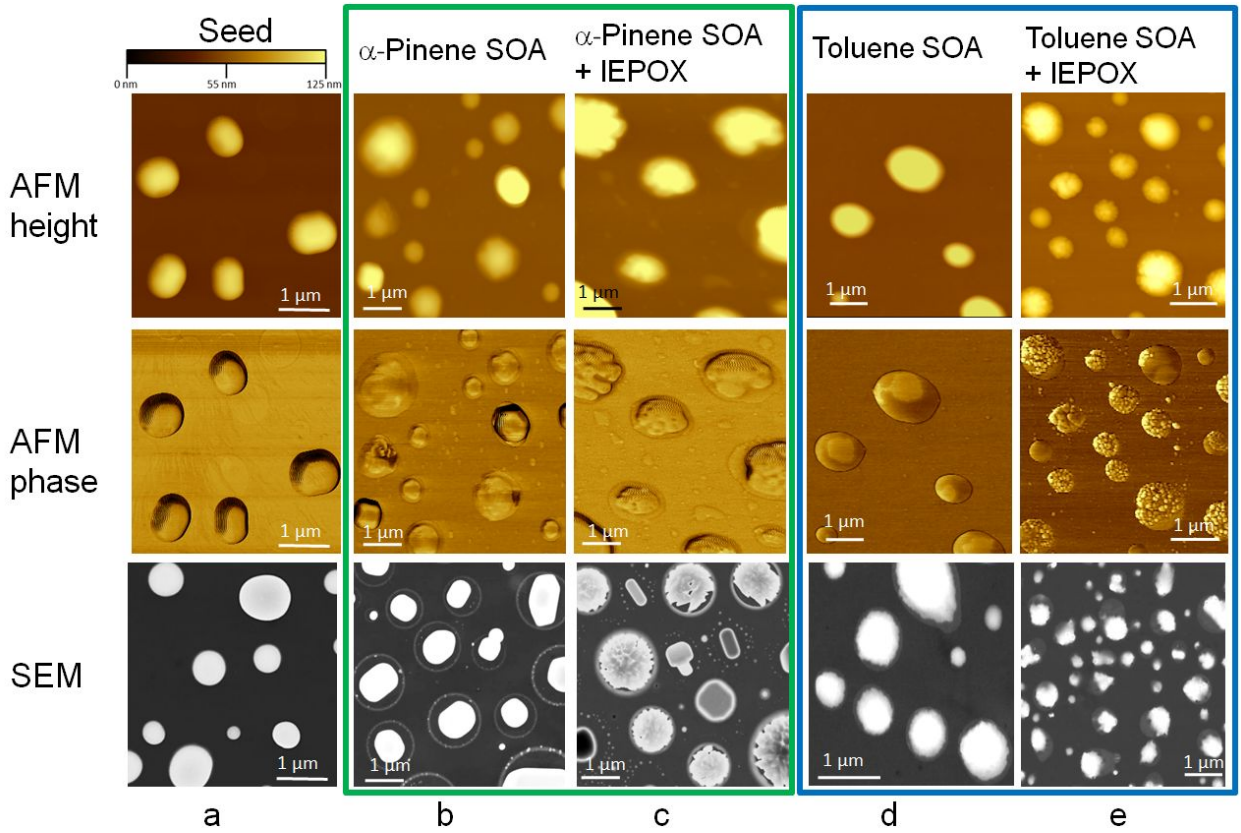

Figure 2. Representative AFM height images (top row), AFM phase images (middle row), and SEM images (bottom row) of seed particles (a), α-pinene SOA/sulfate particles (b), α-pinene SOA/sulfate after IEPOX uptake (c), toluene SOA/sulfate (d), and toluene SOA/sulfate after IEPOX uptake (e). All particles were generated at 50% RH.

To quantify the observed changes in particle morphology and phase state shown in Figure 2, AFM height traces from 10 seed particles, SOA-coated particles, and SOA particles exposed to IEPOX were averaged (Figure 3c and 3d). Acidic ammonium sulfate seed particles had average heights of 70 ± 10 nm, which is in the range of spreading values observed for liquid particles impacted on silicon previously.[87] After coating with α-pinene- or toluene-derived SOA, particle heights increased, indicating particles spread less upon impaction, as depicted in the cartoon in Figure 4a. α-Pinene coated core-shell particles were taller (150 ± 10 nm), on average, than toluene coated core-shell particles (110 ± 10 nm). The increase in particle height after impaction onto substrates is related to particle viscosity because more viscous particles will spread less and will therefore remain taller.[87,91] The particle heights observed here are in agreement with predicted viscosities of the α-pinene (9.3×10^7 Pa s)[7,88] and toluene (7.8×10^4 Pa s)[70,88,89] SOA at 50% RH in previous work.[32,53,70,88,92] The results presented here are only applicable at 50% RH, as toluene SOA has higher viscosity than α-pinene SOA at lower RH.[88] After IEPOX uptake, both types of mixed sulfate-SOA particles were taller and larger in diameter than SOA coated particles. Average particle height of α-pinene SOA + acidic seed particles exposed to IEPOX were 170 ± 10 nm (20 nm taller than α-pinene SOA + acidic seed) and toluene SOA + acidic seed particles exposed to IEPOX were 130 ± 10 nm (20 nm taller than toluene SOA + acidic seed). Representative 3-dimensional AFM images show particle morphology at the three steps in the experiment **(Figure 3a and 3b)**. With the high volume fraction of organic present, the core would not be expected to effloresce at the 30-40% RH values at which the particles were imaged.[62,68] 3D images show particles coated with SOA become taller on the substrate than seed particles. Particle cores become taller after IEPOX uptake while the particle shell appeared flat on the substrate, suggesting the cores are becoming more viscous through IEPOX uptake and core chemistry modification.

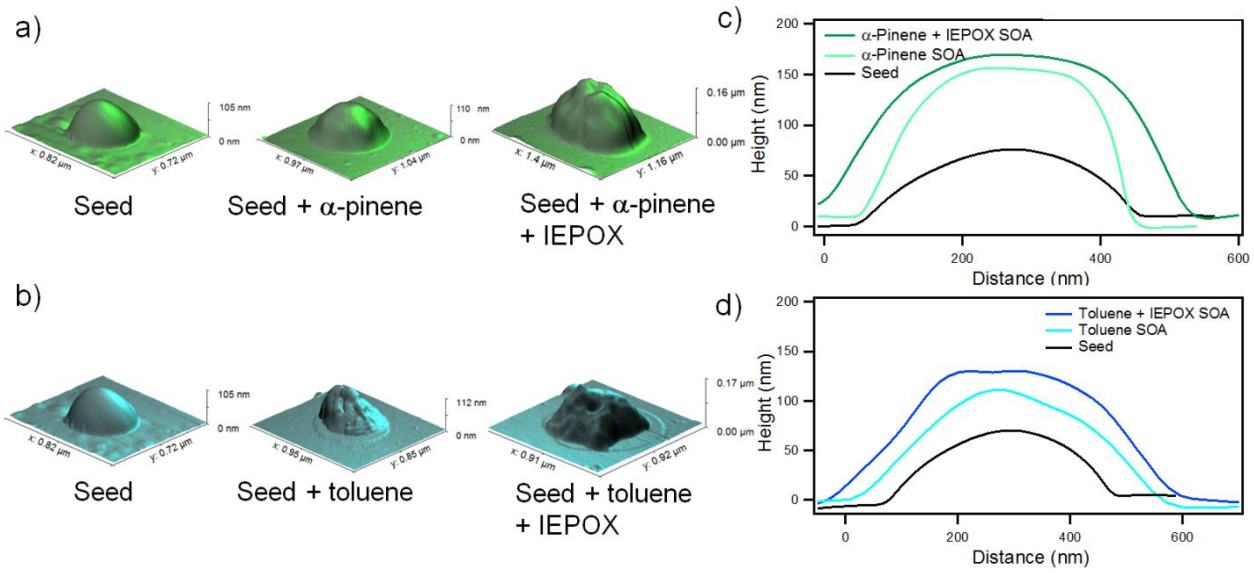

Figure 3. Representative 3D AFM images of a) α-pinene SOA/sulfate and b) toluene SOA/sulfate particles before and after IEPOX uptake. 3D images show flat shells for phase-separated SOA and viscous, tall cores. Average height traces of 10 particles composed of c) α-pinene SOA/sulfate and d) toluene SOA/sulfate before and after IEPOX uptake.

To further investigate changes in particle viscosity and account for differences in particle diameter, spreading ratios were calculated for individual SOA + acidic seed particles using Eq. 2, which compares particle radius to particle height. Particle spreading is used as an indirect measurement of particle viscosity, as more viscous particles will remain taller on the substrate by spreading less and will thus have a lower spreading ratio compared to more liquid-like particles of lower viscosity.[87] Average spreading ratios for ~30 particles per sample measured at 50% RH are shown in Figure 4**.** Seed particles had an average spreading ratio of 6.6 ± 0.7. After coating with α-pinene or toluene SOA, the average spreading ratio decreased to 3.4 ± 0.2 for α-pinene SOA + acidic seed and 3.9 ± 0.4 for toluene SOA + acidic seed particles, and were thus more viscous, in agreement with predictions by Zhang et al.[32] This shift to less spreading upon impaction for phase-separated particles agrees with qualitative observations in Bondy et al.[87] for liquid-liquid phase-separated polyethylene glycol and ammonium sulfate particles. After reactive uptake of IEPOX

leading to altered core morphology, average spreading ratio further decreased to 2.6 ± 0.2 for α-pinene SOA and 3.4 ± 0.7 for toluene SOA particles. Spreading ratios of α-pinene SOA and seed particles generated at 30% RH are shown in Figure S6 and follow similar trends of decreased spreading after coating with α-pinene oxidation products and further decrease in spreading following IEPOX uptake.

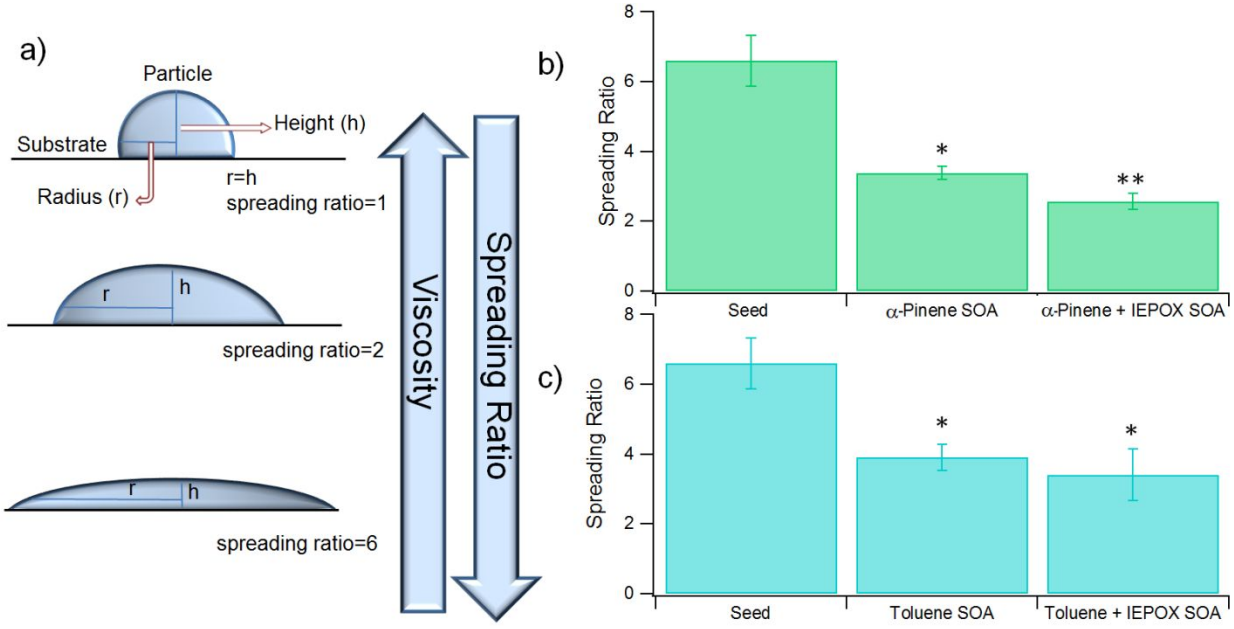

Figure 4. a) Diagrams depicting particle spreading onto substrates. Particle spreading is inversely related to particle viscosity. Bar charts show average spreading ratio of ~30 particles/sample for b) α-pinene SOA/sulfate particles before and after IEPOX uptake and c) toluene SOA/sulfate particles before and after IEPOX uptake. Error bars represent standard error. Single asterisks denote spreading ratios that are statistically different than seed aerosol ($p < 0.05$). The double asterisk denotes spreading ratio that are statistically different than spreading ratio before IEPOX uptake.

To examine the relationship between particle size, composition, and phase separation, particle phase state and d_{ve} of ~500 particles per sample were measured and plotted as histograms (Figure 5). We observed particles under 80 nm (d_{ve}) to have homogeneous composition for all SOA samples, similar to previously published work.[10,57] Before IEPOX uptake, the smallest phase-

separated particles were 160 ± 10 nm (d_{ve}) for α-pinene SOA + acidic seed (mode 570 ± 20 nm) and 127 ± 5 nm (d_{ve}) for toluene SOA + acidic seed (mode 342 ± 5 nm), and most often resulted in a core-shell morphology. This agrees with Fard et al.[93] who stated the most likely morphology for phase-separated atmospheric particles greater than 100 nm was core-shell due to kinetically fast inorganic diffusion, preventing further nucleation after the first inclusion. After IEPOX uptake, the size of the smallest phase-separated particles decreased to 83 ± 3 nm (d_{ve}) for α-pinene SOA (mode 239 ± 3 nm) and 80 ± 3 nm (d_{ve}) for toluene SOA (mode 259 ± 3 nm). When the particle core contains less water and is a more viscous semi-solid, the organic layer becomes less miscible and can initiate a separate phase at smaller particle sizes.[8] The transition regime, the size range where phase-separated and homogeneous particles both exist,[10] became wider for both SOA types after IEPOX uptake, expanding from 150 – 230 nm to 80 – 180 nm after uptake of IEPOX onto α-pinene SOA + acidic seed and from 130 – 280 nm to 80 – 270 nm for toluene SOA + acidic seed after IEPOX uptake. The widening of the transition region, due to greater variability in core composition based on differences in reactive uptake of IEPOX,[32] introduces increased difficulty for predicting phase for particles within these size ranges. Pie chart insets in **Figure 5** show the percent of particles that were phase-separated versus homogeneous. After IEPOX uptake, the percent of phase-separated particles decreased from 67.9 ± 0.6% to 58.8 ± 0.2% for α-pinene SOA and from 68.2 ± 0.2% to 61.6 ± 0.1% for toluene SOA.

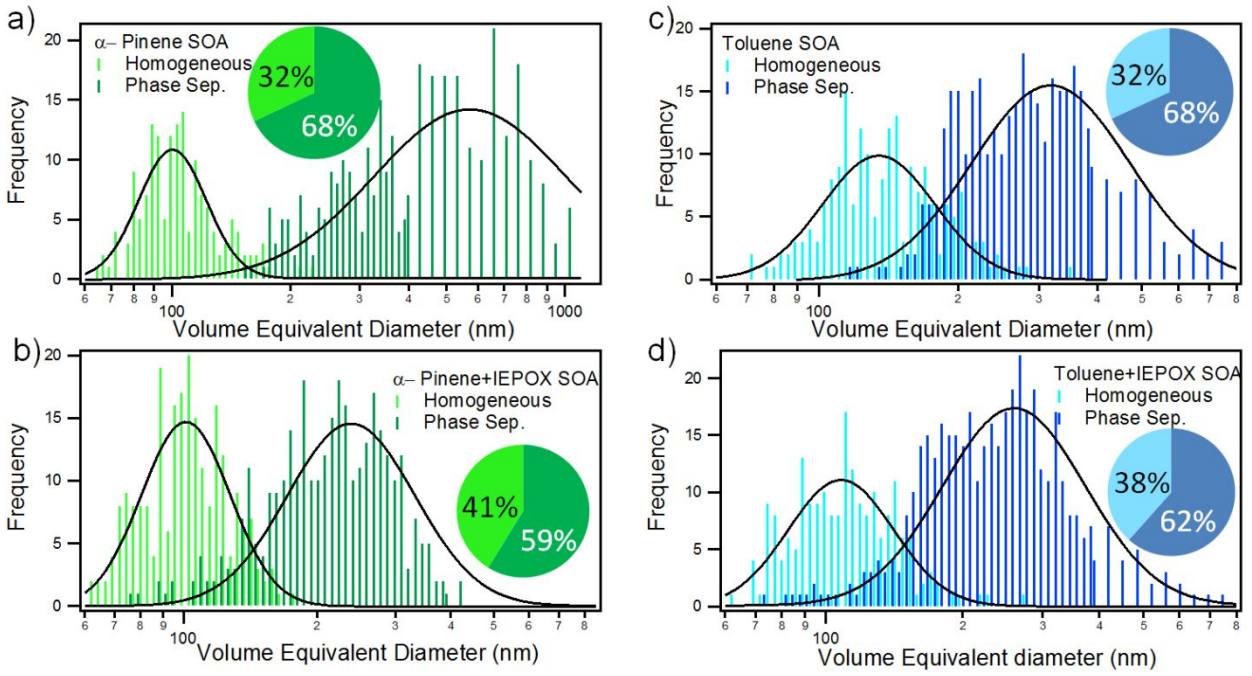

Figure 5. Histograms depicting size-dependent morphology behavior of a) α-pinene SOA/sulfate, b) α-pinene + IEPOX SOA/sulfate, c) toluene SOA/sulfate, and d) toluene + IEPOX SOA/sulfate particles. Lognormal fits show modes at 570 ± 20 nm for phase-separated α-pinene SOA/sulfate, 239 ± 3 nm for phase-separated α-pinene + IEPOX SOA/sulfate, 342 ± 5 nm for phase-separated toluene SOA/sulfate, and 259 ± 3 nm for phase-separated toluene SOA/sulfate. After determining modes, sticks representing phase-separated particles were offset by 25 nm to visualize differences between homogeneous and phase-separated traces. Pie charts represent the percent of particles that were phase-separated versus homogeneous.

Chemical composition plays a key role in determining viscosity, so both α-pinene and toluene SOA-containing particles were analyzed using SEM-EDX for elemental composition and Raman microspectroscopy for functional group composition. Raman spectra of acidic ammonium sulfate seed particles do not show evidence for the presence of organic species (Figure S7), as shown previously.[94,95] Once seed particles were coated with α-pinene or toluene SOA, separate EDX and Raman spectra were taken for the particle core and shell. EDX showed particle cores contained sulfur and oxygen, indicative of sulfate, while particle shells contained primarily carbon and oxygen, indicative of α-pinene or toluene SOA **(Figure 6)**. Sulfur is clearly discernable and located primarily in the core of particles. Raman spectra show the broad ν(N-H) region around

3200 cm^{-1} indicating ammonium and a mode for $\nu_s(SO_4^{2-})$ was observed at 976 cm^{-1} in the particle core before IEPOX uptake (Figure 7).[96-101] Peaks in the ν(C-H) region between 2800-3000 cm^{-1} indicate organic materials in the shell of α-pinene and toluene SOA-coated acidic seed particles. Specifically, methyl $\nu(CH_3)$ and methylene $\nu(CH_2)$ symmetric and anti-symmetric stretches were detected, along with modes in the organic fingerprint region which are listed in the Supporting Information (Table S1). Differences in composition between particle core and shell for both SOA types shows that the coating of α-pinene or toluene SOA creates chemically distinct phases with a primarily inorganic core and organic shell, instead of homogeneously mixed particles. After IEPOX uptake, EDX spectra show particle cores contained carbon for both types of SOA, suggesting IEPOX reaction forming organic species, possibly organosulfur compounds (i.e., organosulfates and oligomers thereof), within the particle core. After IEPOX uptake, SOA cores contained methyl $\nu(CH_3)$ and methylene $\nu(CH_2)$ symmetric and anti-symmetric stretches in the Raman spectra. Particle cores also showed signs of organosulfate formation with peaks around 1060 cm^{-1} in the Raman spectra, indicative of $\nu_s(RO\text{-}SO_3)$.[46] Peaks indicative of organosulfates were not observed in the shell for either α-pinene and toluene SOA after IEPOX uptake indicating that the shells did not mix with the core as it solidified. Future work will investigate conditions for organosulfate formation in various types of SOA across a range of RH conditions.[36,45,48,50,102-104]

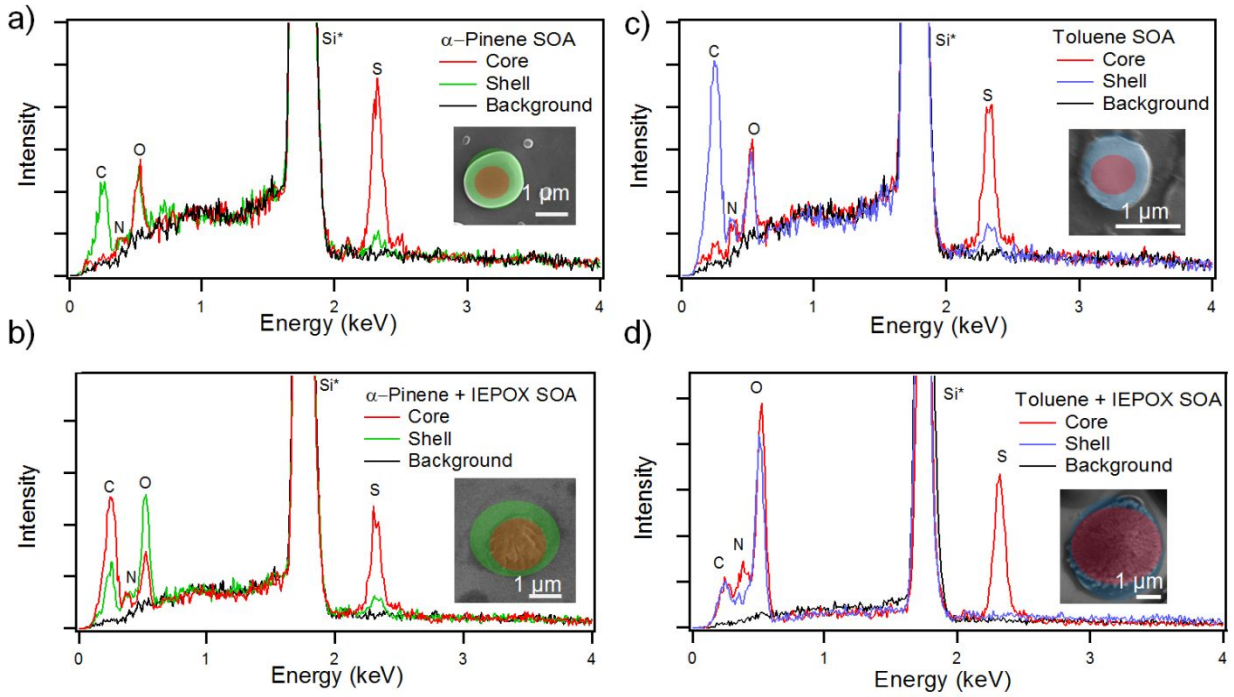

Figure 6. Representative SEM images and EDX spectra of a) α-pinene SOA/sulfate particles, b) α-pinene SOA/sulfate + IEPOX particles, c) toluene SOA/sulfate particles, and d) toluene SOA/sulfate + IEPOX particles showing differences between core and shell composition. Elements with asterisk denote contribution from substrate. Images were colored to easily identify phase-separated morphology. Unedited images are shown in the Supporting Information (Figure S8).

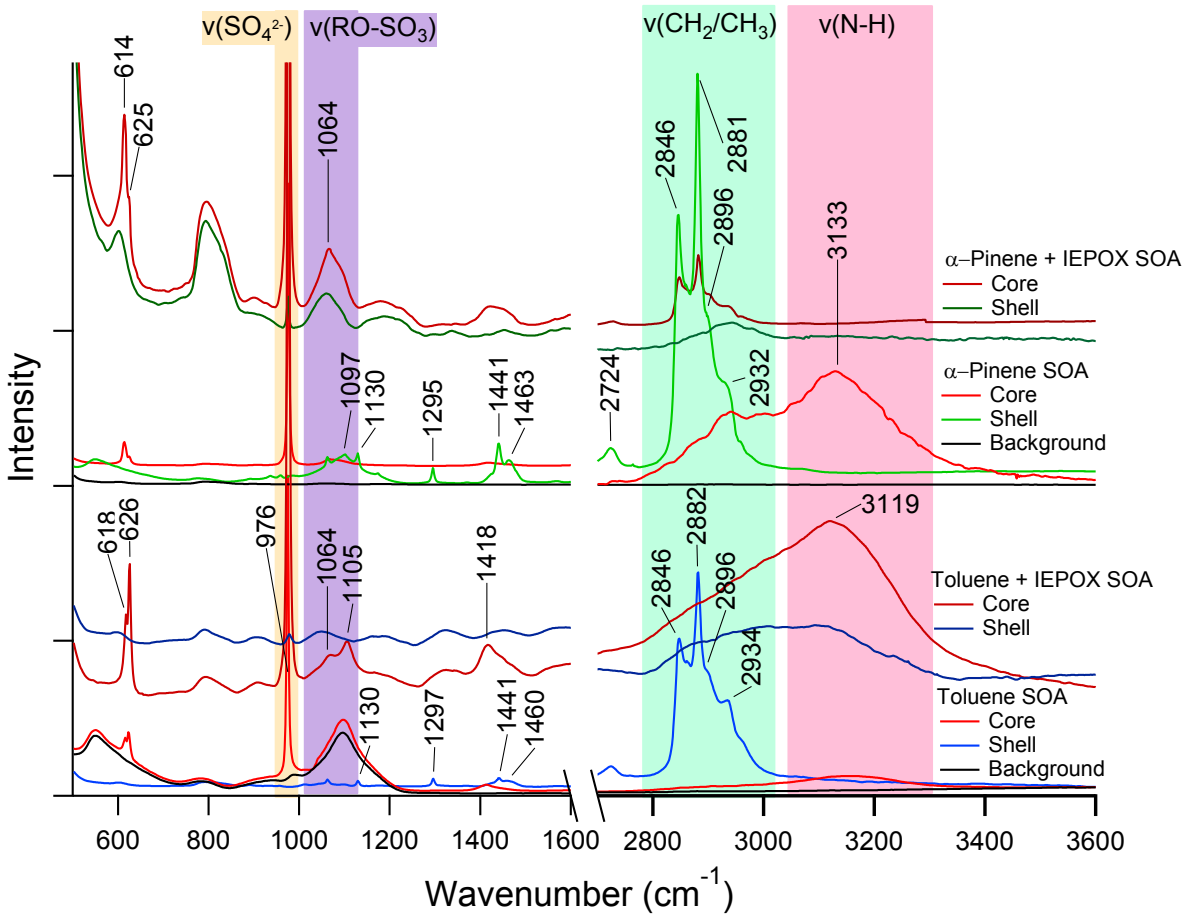

Figure 7. Representative Raman spectra of α-pinene SOA/sulfate particles before and after IEPOX reactive uptake (top) and toluene SOA/sulfate particles before and after IEPOX reactive uptake (bottom) showing differences between core and shell composition.

Atmospheric Implications

The existence of liquid-liquid phase-separated particles in the ambient atmosphere and their role in modifying reactive uptake has important consequences for SOA formation and PM concentrations. Recent flow tube studies have shown that IEPOX uptake can be reduced by liquid-liquid phase separations involving coatings of α-pinene SOA around an acidic aqueous core rich in sulfate.[32] This is true even with a pH of 1.5 for the core, typical of pH values for the southeast United States (0-2).[60,105] Chamber studies have shown that inorganic sulfate can rapidly be converted into organosulfates after reaction with IEPOX,[106] which are quite viscous. The

atmospheric implications of the results from this study are that the core of phase-separated submicron particles can be converted from aqueous-inorganic to viscous organics, such as IEPOX-derived organosulfates, which can further inhibit SOA formation. This viscous core formation occurs within acidic inorganic particles coated with both α-pinene (biogenic) and toluene (anthropogenic) SOA. That the increased core viscosity occurs on the timescale of flowtube experiments (< 1 min) indicates that the α-pinene and toluene coatings were not sufficiently viscous at 50% RH to fully inhibit IEPOX uptake and the subsequent rapid formation of viscous organosulfates in the core. The increase in core viscosity and thus diffusion and mixing timescales likely limits additional reactive uptake of IEPOX, since acidic particles (pH = 1.5) have been shown to form organosulfates that almost completely shut off IEPOX uptake within 40 hours of simulated atmospheric aging.[106] The prevalence of phase separated and viscous particles may impact atmospheric model predictions of IEPOX-derived SOA, as many of these models do not consider the kinetic limitations of phase-separated particles on multiphase chemical processes yielding SOA.[107] Recent modeling has shown that α-pinene SOA coatings around acidic cores can decrease SOA formation by 33%, even at 55-80% RH,[108] but the impact of transforming an aqueous acidic core to a diffusion limited viscous core could have an even larger effect, but has not yet been evaluated. The increased viscosity and morphologies observed could also impact the CCN and INP properties of these aerosols.[3,5,109] Therefore, further studies are needed to improve understanding of phase separation and viscosity in flowtube, chamber, and ambient particles of different and more complex compositions and at different atmospheric conditions.

Supporting Information

The Supporting Information is available free of charge via http://pubs.acs.org. Description of experimental parameters (Text S1), schematic of experimental setup (Figure S1), AFM images of

α-pinene SOA rehumidified to the RH at which they were generated (Figure S2), SEM images of ambient particles containing core-shell morphology (Figure S3), SEM and AFM images of α-pinene SOA generated at 30% RH (Figure S4), SEM images of toluene SOA generated at 30% RH (Figure S5), spreading ratios of α-pinene SOA generated at 30% RH (Figure S6), SEM image with EDX and Raman spectra of seed particle (Figure S7), uncolored SEM images of SOA particles shown in Figure 6 (Figure S8), Raman mode assignments and intensity classification (Table S1).

Acknowledgments: This work was supported by collaborative grants from the National Science Foundation (NSF) Grant No. AGS-1506768 (Ault) and No. AGS-1703535 (Surratt). NSF grant No. AGS-1537446 (Lambe) supported the use of the PAM. Yue Zhang was supported by the NSF Postdoctoral Fellowship under AGS Grant No. 1524731.The authors acknowledge the University of Michigan College of Engineering for financial support of the Michigan Center for Materials Characterization (MC^2), including partially subsidizing use of the electron microscopy instruments and staff assistance. AFM was performed at the Scanning Probe Microscopy facility in the Department of Chemistry at the University of Michigan.

References

1. Pöschl, U., Atmospheric aerosols: Composition, transformation, climate and health effects. *Atmos. Chem.* **2005,** *44*, 7520 – 7540.
2. Prather, K. A.; Hatch, C. D.; Grassian, V. H., Analysis of atmospheric aerosols. *Annu. Rev. Anal. Chem.* **2008,** *1*, 485-514.
3. Knopf, D. A.; Alpert, P. A.; Wang, B., The role of organic aerosol in atmospheric ice nucleation: a review. *ACS Earth Space Chem.* **2018,** *2*, (3), 168-202.
4. Ault, A.; Axson, J., Atmospheric aerosol chemistry: spectroscopic and microscopic advances. *Anal. Chem.* **2016,** *89*, 430-452.
5. Riemer, N., Ault, A. P., West, M., Craig, R. L., Curtis, J. H., Aerosol mixing state: measurements,modeling, and impacts. *Review of Geophysics* **2019,** *57*, 1-63.
6. Saukko, E.; Lambe, A. T.; Massoli, P.; Koop, T.; Wright, J. P.; Croasdale, D. R.; Pedernera, D. A.; Onasch, T. B.; Laaksonen, A.; Davidovits, P.; Worsnop, D. R.; Virtanen, A., Humidity-dependent phase state of SOA particles from biogenic and anthropogenic precursors. *Atmos. Chem. Phys* **2012,** *12*, (16), 7517-7529.
7. Zhang, Y.; Sanchez, M. S.; Douet, C.; Wang, Y.; Bateman, A. P.; Gong, Z.; Kuwata, M.; Renbaum-Wolff, L.; Sato, B. B.; Liu, P. F.; Bertram, A. K.; Geiger, F. M.; Martin, S. T., Changing shapes and implied viscosities of suspended submicron particles. *Atmos. Chem. Phys* **2015,** *15*, (14), 7819-7829.
8. You, Y.; Smith, M. L.; Song, M.; Martin, S. T.; Bertram, A. K., Liquid–liquid phase separation in atmospherically relevant particles consisting of organic species and inorganic salts. *Int. Rev. Phys. Chem.* **2014,** *33*, (1), 43-77.
9. You, Y.; Renbaum-Wolff, L.; Bertram, A. K., Liquid–liquid phase separation in particles containing organics mixed with ammonium sulfate, ammonium bisulfate, ammonium nitrate or sodium chloride. *Atmos. Chem. Phys* **2013,** *13*, (23), 11723-11734.
10. Altaf, M. B.; Freedman, M. A., Effect of drying rate on aerosol particle morphology. *J. Phys. Chem. Lett.* **2017,** *8*, 3613-3618.
11. Freedman, M. A., Phase separation in organic aerosol. *Chem. Soc. Rev.* **2017,** *46*, 7694-7705.
12. Freedman, M. B., Baustian, K. J.,Wise, M. E., Tolbert, M. A., Characterizing the morphology of organic aerosols at ambient temperature and pressure. *Anal. Chem.* **2010,** *82*, 7965–7972.
13. Slade, J. H.; Ault, A. P.; Bui, A. T.; Ditto, J. C.; Lei, Z.; Bondy, A. L.; Olson, N. E.; Cook, R. D.; Desrochers, S. J.; Harvey, R. M.; Erickson, M. H.; Wallace, H. W.; Alvarez, S. L.; Flynn, J. H.; Boor, B. E.; Petrucci, G. A.; Gentner, D. R.; Griffin, R. J.; Shepson, P. B., Bouncier particles at night: biogenic secondary organic aerosol chemistry and sulfate drive diel variations in the aerosol phase in a mixed forest. *Environ. Sci. Technol.* **2019,** *53*, 4977-4987.
14. You, Y.; Renbaum-Wolff, L.; Carreras-Sospedra, M.; Hanna, S. J.; Hiranuma, N.; Kamal, S.; Smith, M. L.; Zhang, X.; Weber, R. J.; Shilling, J. E.; Dabdub, D.; Martin, S. T.; Bertram, A. K., Images reveal that atmospheric particles can undergo liquid-liquid phase separations. *Proc. Natl. Acad. Sci. U. S. A.* **2012,** *109*, (33), 13188–13193.
15. Bondy, A. L.; Bonanno, D.; Moffet, R. C.; Wang, B.; Laskin, A.; Ault, A. P., The diverse chemical mixing state of aerosol particles in the southeastern United States. *Atmos. Chem. Phys* **2018,** *18*, (16), 12595-12612.
16. Carlton, A. G., Wiedinmyer, C.,Kroll, J. H. , A review of Secondary Organic Aerosol (SOA) formation from isoprene. *Atmos. Chem. Phys* **2009,** *9*, 4987–5005.

17. Guenther, A., Karl, T.,Harley, P., Wiedinmyer, C., Palmer, P. I., Geron, C., Estimates of global terrestrial isoprene emissions using MEGAN (Model of Emissions of Gases and Aerosols from Nature). *Atmos. Chem. Phys* **2006,** *6*, 3181–3210.
18. Renbaum-Wolff, L.; Grayson, J. W.; Bateman, A. P.; Kuwata, M.; Sellier, M.; Murray, B. J.; Shilling, J. E.; Martin, S. T.; Bertram, A. K., Viscosity of alpha-pinene secondary organic material and implications for particle growth and reactivity. *Proc. Natl. Acad. Sci. U. S. A.* **2013,** *110*, (20), 8014-8019.
19. Beauregard, D., *Locating and estimating air emissions from sources of toluene*. Office of Air Quality Planning and Standards, United States Environmental Protection Agency, EPA: Research Triangle Park, NC, 1994.
20. Hallquist, M., Wenger,J. C., Baltensperger, U., Rudich, Y., Simpson, D., Claeys, M., Dommen, J. , ; Donahue, N. M., George, C., Goldstein, A. H., Hamilton, J. F., Herrmann, H., Hoffmann, T., Iinuma, Y.,; Jang, M., Jenkin, M. E., Jimenez, J. L., Kiendler-Scharr, A., Maenhaut, W., McFiggans, G., Mentel, Th. F.,; Monod, A., Prevot, A. S. H., Seinfeld,J. H., Surratt, J. D., Szmigielski, R., Wildt, J., The formation, properties, and impacts of secondary organic aerosol: current and emerging issues. *Atmos. Chem. Phys* **2009,** *9*, 5155–5236.
21. Zhang, H., Lindsay D. Yee, Ben H. Lee, Michael P. Curtis, David R.; Worton, G. I.-V., John H. Offenberg, Michael Lewandowski, Tadeusz; E. Kleindienst, M. R. B., Amara L. Holder, William A. Lonneman, Kenneth S.; Docherty, M. J., Havala O. T. Pye, Weiwei Hu, Douglas A. Day, Pedro; Campuzano-Jost, J. L. J., Hongyu Guo, Rodney J. Weber, Joost de Gouw, Abigail R. Koss, Eric S. Edgerton, William Brune, Claudia Mohr, Felipe D. Lopez-; Hilfiker, A. L., Nathan M. Kreisberg, Steve R. Spielman, Susanne V. Hering, Kevin; R. Wilson, J. A. T., Allen H. Goldstein, Monoterpenes are the largest source of summertime organic aerosol in the Southeastern United States. *Proc. Natl. Acad. Sci. U. S. A.* **2018,** *115*, 2038-2043.
22. Guenther, A. B.; Jiang, X.; Heald, C. L.; Sakulyanontvittaya, T.; Duhl, T.; Emmons, L. K.; Wang, X., The Model of Emissions of Gases and Aerosols from Nature version 2.1 (MEGAN2.1): an extended and updated framework for modeling biogenic emissions. *Geosci. Mod. Devel.* **2012,** *5*, (6), 1471-1492.
23. Bates, K. H.; Crounse, J. D.; St Clair, J. M.; Bennett, N. B.; Nguyen, T. B.; Seinfeld, J. H.; Stoltz, B. M.; Wennberg, P. O., Gas phase production and loss of isoprene epoxydiols. *J Phys Chem A.* **2014,** *118*, (7), 1237-1246.
24. Paulot, F.; Crounse, J. D.; Kjaergaard, H. G.; Kurten, A.; St Clair, J. M.; Seinfeld, J. H.; Wennberg, P. O., Unexpected epoxide formation in the gas-phase photooxidation of isoprene. *Science* **2009,** *325*, (5941), 730-733.
25. Riva, M.; Budisulistiorini, S. H.; Zhang, Z.; Gold, A.; Thornton, J. A.; Turpin, B. J.; Surratt, J. D., Multiphase reactivity of gaseous hydroperoxide oligomers produced from isoprene ozonolysis in the presence of acidified aerosols. *Atmos. Env.* **2017,** *152*, 314-322.
26. Gaston, C. J.; Riedel, T. P.; Zhang, Z.; Gold, A.; Surratt, J. D.; Thornton, J. A., Reactive uptake of an isoprene-derived epoxydiol to submicron aerosol particles. *Environ. Sci. Technol.* **2014,** *48*, (19), 11178-11186.
27. Riedel, T. P.; Lin, Y.-H.; Budisulistiorini, S. H.; Gaston, C. J.; Thornton, J. A.; Zhang, Z.; Vizuete, W.; Gold, A.; Surratt, J. D., Heterogeneous reactions of isoprene-derived epoxides: reaction probabilities and molar secondary organic aerosol yield estimates. *Environ. Sci. Technol. Lett.* **2015,** *2*, (2), 38-42.

28. Jang, M., Czoschke, N. M., Lee, S., Kamens, R. M., Heterogeneous atmospheric aerosol production by acid- catalyzed particle-phase reactions. *Science* **2002,** *298*, 814-817.
29. Czoschke, N. M., Jang, M., Kamens, R. M., Effect of acidic seed on biogenic secondary organic aerosol growth. *Atmos. Env.* **2003,** *37*, (30), 4287-4299.
30. Budisulistiorini, S. H.; Baumann, K.; Edgerton, E. S.; Bairai, S. T.; Mueller, S.; Shaw, S. L.; Knipping, E. M.; Gold, A.; Surratt, J. D., Seasonal characterization of submicron aerosol chemical composition and organic aerosol sources in the southeastern United States: Atlanta, Georgia,and Look Rock, Tennessee. *Atmos. Chem. Phys* **2016,** *16*, (8), 5171-5189.
31. Hu, W. W.; Campuzano-Jost, P.; Palm, B. B.; Day, D. A.; Ortega, A. M.; Hayes, P. L.; Krechmer, J. E.; Chen, Q.; Kuwata, M.; Liu, Y. J.; de Sá, S. S.; McKinney, K.; Martin, S. T.; Hu, M.; Budisulistiorini, S. H.; Riva, M.; Surratt, J. D.; St. Clair, J. M.; Isaacman-Van Wertz, G.; Yee, L. D.; Goldstein, A. H.; Carbone, S.; Brito, J.; Artaxo, P.; de Gouw, J. A.; Koss, A.; Wisthaler, A.; Mikoviny, T.; Karl, T.; Kaser, L.; Jud, W.; Hansel, A.; Docherty, K. S.; Alexander, M. L.; Robinson, N. H.; Coe, H.; Allan, J. D.; Canagaratna, M. R.; Paulot, F.; Jimenez, J. L., Characterization of a real-time tracer for isoprene epoxydiols-derived secondary organic aerosol (IEPOX-SOA) from aerosol mass spectrometer measurements. *Atmos. Chem. Phys* **2015,** *15*, (20), 11807-11833.
32. Zhang, Y.; Chen, Y.; Lambe, A. T.; Olson, N. E.; Lei, Z.; Craig, R. L.; Zhang, Z.; Gold, A.; Onasch, T. B.; Jayne, J. T.; Worsnop, D. R.; Gaston, C. J.; Thornton, J. A.; Vizuete, W.; Ault, A. P.; Surratt, J. D., Effect of the aerosol-phase state on secondary organic aerosol formation from the reactive uptake of isoprene-derived epoxydiols (IEPOX). *Environ. Sci. Technol. Lett.* **2018,** *5*, 167-174.
33. Fuzzi, S., Andreae, M. O., Huebert, B. J., Kulmala, M., Bond,T. C., Boy, M.,Doherty, S. J., Guenther, A., Kanakidou ,M., Kawamura, K., Kerminen, V. M., Lohmann, U., Russell, L.M., Poschl, U. , Critical assessment of the current state of scientific knowledge, terminology, and research needs concerning the role of organic aerosols in the atmosphere, climate, and global change. *Atmos. Chem. Phys* **2006,** *6*, 2017–2038.
34. Reid, J. P.; Dennis-Smither, B. J.; Kwamena, N. O.; Miles, R. E.; Hanford, K. L.; Homer, C. J., The morphology of aerosol particles consisting of hydrophobic and hydrophilic phases: hydrocarbons, alcohols and fatty acids as the hydrophobic component. *Phys. Chem. Chem. Phys.* **2011,** *13*, (34), 15559-15572.
35. Erdakos, G. B.; Chang, E. I.; Pankow, J. F.; Seinfeld, J. H., Prediction of activity coefficients in liquid aerosol particles containing organic compounds, dissolved inorganic salts, and water—Part 3: Organic compounds, water, and ionic constituents by consideration of short-, mid-, and long-range effects using X-UNIFAC.3. *Atmos. Env.* **2006,** *40*, (33), 6437-6452.
36. Riva, M.; Bell, D. M.; Hansen, A. M.; Drozd, G. T.; Zhang, Z.; Gold, A.; Imre, D.; Surratt, J. D.; Glasius, M.; Zelenyuk, A., Effect of organic coatings, humidity and aerosol acidity on multiphase chemistry of isoprene epoxydiols. *Environ. Sci. Technol.* **2016,** *50*, (11), 5580-5588.
37. Shiraiwa, M.; Zuend, A.; Bertram, A. K.; Seinfeld, J. H., Gas-particle partitioning of atmospheric aerosols: interplay of physical state, non-ideal mixing and morphology. *Phys. Chem. Chem. Phys.* **2013,** *15*, (27), 11441-11453.
38. Renbaum-Wolff, L.; Song, M.; Marcolli, C.; Zhang, Y.; Liu, P. F.; Grayson, J. W.; Geiger, F. M.; Martin, S. T.; Bertram, A. K., Observations and implications of liquid–liquid phase separation at high relative humidities in secondary organic material produced by a-pinene ozonolysis without inorganic salts. *Atmos. Chem. Phys* **2016,** *16*, (12), 7969-7979.

39. Chang, E. I.; Pankow, J. F., Prediction of activity coefficients in liquid aerosol particles containing organic compounds, dissolved inorganic salts, and water—Part 2: Consideration of phase separation effects by an X-UNIFAC model. *Atmos. Environ.* **2006,** *40*, (33), 6422-6436.
40. Zuend, A.; Seinfeld, J. H., Modeling the gas-particle partitioning of secondary organic aerosol: the importance of liquid-liquid phase separation. *Atmos. Chem. Phys* **2012,** *12*, (9), 3857-3882.
41. Brunamonti, S., Krieger, U. K., Marcolli, C., Peter, T., Redistribution of black carbon in aerosol particles undergoing liquid-liquid phase separation. *Geophys. Res. Lett.* **2015,** *42*, 2532–2539.
42. Lienhard, D. M.; Huisman, A. J.; Krieger, U. K.; Rudich, Y.; Marcolli, C.; Luo, B. P.; Bones, D. L.; Reid, J. P.; Lambe, A. T.; Canagaratna, M. R.; Davidovits, P.; Onasch, T. B.; Worsnop, D. R.; Steimer, S. S.; Koop, T.; Peter, T., Viscous organic aerosol particles in the upper troposphere: diffusivity-controlled water uptake and ice nucleation? *Atmos. Chem. Phys* **2015,** *15*, (23), 13599-13613.
43. Virtanen, A.; Joutsensaari, J.; Koop, T.; Kannosto, J.; Yli-Pirila, P.; Leskinen, J.; Makela, J. M.; Holopainen, J. K.; Poschl, U.; Kulmala, M.; Worsnop, D. R.; Laaksonen, A., An amorphous solid state of biogenic secondary organic aerosol particles. *Nature* **2010,** *467*, (7317), 824-827.
44. Pajunoja, A.; Malila, J.; Hao, L.; Joutsensaari, J.; Lehtinen, K. E. J.; Virtanen, A., Estimating the viscosity range of SOA particles based on their coalescence time. *Aerosol. Sci. Technol.* **2013,** *48*, (2), i-iv.
45. Surratt, J. D.; Chan, A. W.; Eddingsaas, N. C.; Chan, M.; Loza, C. L.; Kwan, A. J.; Hersey, S. P.; Flagan, R. C.; Wennberg, P. O.; Seinfeld, J. H., Reactive intermediates revealed in secondary organic aerosol formation from isoprene. *Proc. Natl. Acad. Sci. U. S. A.* **2010,** *107*, (15), 6640-6645.
46. Bondy, A. L.; Craig, R. L.; Zhang, Z.; Gold, A.; Surratt, J. D.; Ault, A. P., Isoprene-derived organosulfates: vibrational mode analysis by Raman spectroscopy, acidity-dependent spectral modes, and observation in individual atmospheric particles. *J. Phys. Chem. A* **2018,** *122*, (1), 303-315.
47. Budisulistiorini, S. H.; Nenes, A.; Carlton, A. M. G.; Surratt, J. D.; McNeill, V. F.; Pye, H. O. T., Simulating aqueous-phase isoprene-epoxydiol (IEPOX) secondary organic aerosol production during the 2013 Southern Oxidant and Aerosol Study (SOAS). *Environ. Sci. Technol.* **2016,** *51*, 5026-5034.
48. Surratt, J. D., Gomez-Gonzalez, Y., Chan, Arthur W. H.,Vermeylen, Reinhilde. Shahgholi, Mona. Kleindienst,Tadeusz E., Edney, Edward O., Offenberg, John H., Lewandowski, Michael. Jaoui, Mohammed. Maenhaut, Willy. Claeys, Magda.Flagan, Richard C., Seinfeld, John H. , Organosulfate formation in biogenic secondary organic aerosol *J. Phys. Chem. A* **2008,** *112*, 8345–8378.
49. Surratt, J. D.; Murphy, S. M.; Kroll, J. H.; Ng, N. L.; Hildebrandt, L.; Sorooshian, A.; Szmigielski, R.; Vermeylen, R.; Maenhaut, W.; Claeys, M.; Flagan, R. C.; Seinfeld, J. H., Chemical composition of secondary organic aerosol formed from the photooxidation of isoprene. *J. Phys. Chem. A* **2006,** *110*, (31), 9665-9690.
50. Lin, Y. H.; Zhang, Z.; Docherty, K. S.; Zhang, H.; Budisulistiorini, S. H.; Rubitschun, C. L.; Shaw, S. L.; Knipping, E. M.; Edgerton, E. S.; Kleindienst, T. E.; Gold, A.; Surratt, J. D., Isoprene epoxydiols as precursors to secondary organic aerosol formation: acid-catalyzed

reactive uptake studies with authentic compounds. *Environ. Sci. Technol.* **2012,** *46*, (1), 250-258.
51. Lin, Y. H.; Budisulistiorini, S. H.; Chu, K.; Siejack, R. A.; Zhang, H.; Riva, M.; Zhang, Z.; Gold, A.; Kautzman, K. E.; Surratt, J. D., Light-absorbing oligomer formation in secondary organic aerosol from reactive uptake of isoprene epoxydiols. *Environ. Sci. Technol.* **2014,** *48*, (20), 12012−12021.
52. Hosny, N. A.; Fitzgerald, C.; Tong, C.; Kalberer, M.; Kuimova, M. K.; Pope, F. D., Fluorescent lifetime imaging of atmospheric aerosols: a direct probe of aerosol viscosity. *Faraday Discuss.* **2013,** *165*, 343.
53. Shiraiwa, M.; Li, Y.; Tsimpidi, A. P.; Karydis, V. A.; Berkemeier, T.; Pandis, S. N.; Lelieveld, J.; Koop, T.; Poschl, U., Global distribution of particle phase state in atmospheric secondary organic aerosols. *Nature Comm.* **2017,** *8*, 15002.
54. Booth, A. M.; Murphy, B.; Riipinen, I.; Percival, C. J.; Topping, D. O., Connecting bulk viscosity measurements to kinetic limitations on attaining equilibrium for a model aerosol composition. *Environ. Sci. Technol.* **2014,** *48*, (16), 9298−9305.
55. Berkemeier, T.; Shiraiwa, M.; Pöschl, U.; Koop, T., Competition between water uptake and ice nucleation by glassy organic aerosol particles. *Atmos. Chem. Phys* **2014,** *14*, (22), 12513-12531.
56. Shrestha, M.; Zhang, Y.; Upshur, M. A.; Liu, P.; Blair, S. L.; Wang, H. F.; Nizkorodov, S. A.; Thomson, R. J.; Martin, S. T.; Geiger, F. M., On surface order and disorder of alpha-pinene-derived secondary organic material. *J. Phys. Chem. A* **2014,** *119*, (19), 4609−4617.
57. Veghte, D. P.; Altaf, M. B.; Freedman, M. A., Size dependence of the structure of organic aerosol. *J. Am. Chem. Soc.* **2013,** *135*, (43), 16046−16049.
58. Kwamena, N. O. A., Buajarern, J., Reid, J. P., Equilibrium morphology of mixed organic/inorganic/aqueous aerosol droplets: investigating the effect of relative humidity and surfactants. *J. Phys. Chem. A* **2010,** *114*, 5787–5795.
59. Gorkowski, K.; Donahue, N. M.; Sullivan, R. C., Emulsified and liquid-liquid phase separated states of alpha-pinene secondary organic aerosol determined using aerosol optical tweezers. *Environ. Sci. Technol.* **2017,** *51*, 12154-12163.
60. Guo, H.; Xu, L.; Bougiatioti, A.; Cerully, K. M.; Capps, S. L.; Hite, J. R.; Carlton, A. G.; Lee, S. H.; Bergin, M. H.; Ng, N. L.; Nenes, A.; Weber, R. J., Fine-particle water and pH in the southeastern United States. *Atmos. Chem. Phys* **2015,** *15*, (9), 5211-5228.
61. Pajunoja, A.; Lambe, A. T.; Hakala, J.; Rastak, N.; Cummings, M. J.; Brogan, J. F.; Hao, L.; Paramonov, M.; Hong, J.; Prisle, N. L.; Malila, J.; Romakkaniemi, S.; Lehtinen, K. E. J.; Laaksonen, A.; Kulmala, M.; Massoli, P.; Onasch, T. B.; Donahue, N. M.; Riipinen, I.; Davidovits, P.; Worsnop, D. R.; Petäjä, T.; Virtanen, A., Adsorptive uptake of water by semisolid secondary organic aerosols. *Geophys. Res. Lett.* **2015,** *42*, (8), 3063-3068.
62. Bertram, A. K.; Martin, S. T.; Hanna, S. J.; Smith, M. L.; Bodsworth, A.; Chen, Q.; Kuwata, M.; Liu, A.; You, Y.; Zorn, S. R., Predicting the relative humidities of liquid-liquid phase separation, efflorescence, and deliquescence of mixed particles of ammonium sulfate, organic material, and water using the organic-to-sulfate mass ratio of the particle and the oxygen-to-carbon elemental ratio of the organic component. *Atmos. Chem. Phys* **2011,** *11*, (21), 10995-11006.
63. Ciobanu, V. G.; Marcolli, C.; Krieger, U. K.; Weers, U.; Peter, T., Liquid-liquid phase separation in mixed organic/inorganic aerosol particles. *The journal of physical chemistry. A* **2009,** *113*, (41), 10966-10978.

64. Song, M.; Liu, P.; Martin, S. T.; Bertram, A. K., Liquid–liquid phase separation in particles containing secondary organic material free of inorganic salts. *Atmos. Chem. Phys.* **2017,** *17*, (18), 11261-11271.
65. Lehtipalo, K.; Sipilä, M.; Junninen, H.; Ehn, M.; Berndt, T.; Kajos, M. K.; Worsnop, D. R.; Petäjä, T.; Kulmala, M., Observations of nano-CN in the nocturnal boreal forest. *Aerosol. Sci. Technol.* **2011,** *45*, (4), 499-509.
66. Prisle, N. L.; Engelhart, G. J.; Bilde, M.; Donahue, N. M., Humidity influence on gas-particle phase partitioning of α-pinene + O3 secondary organic aerosol. *Geophys. Res. Lett.* **2010,** *37*, (1), L01802.
67. Vaden, T. D.; Song, C.; Zaveri, R. A.; Imre, D.; Zelenyuk, A., Morphology of mixed primary and secondary organic particles and the adsorption of spectator organic gases during aerosol formation. *Proc. Natl. Acad. Sci. U. S. A.* **2010,** *107*, (15), 6658–6663.
68. Smith, M. L.; Bertram, A. K.; Martin, S. T., Deliquescence, efflorescence, and phase miscibility of mixed particles of ammonium sulfate and isoprene-derived secondary organic material. *Atmos. Chem. Phys.* **2012,** *12*, (20), 9613-9628.
69. Smith, M. L.; Kuwata, M.; Martin, S. T., Secondary organic material produced by the dark ozonolysis of α-pinene minimally affects the deliquescence and efflorescence of ammonium sulfate. *Aerosol Sci. Technol.* **2011,** *45*, (2), 244-261.
70. Song, M.; Liu, P. F.; Hanna, S. J.; Zaveri, R. A.; Potter, K.; You, Y.; Martin, S. T.; Bertram, A. K., Relative humidity-dependent viscosity of secondary organic material from toluene photo-oxidation and possible implications for organic particulate matter over megacities. *Atmos. Chem. Phys* **2016,** *16*, (14), 8817-8830.
71. Craig, R. L.; Peterson, P. K.; Nandy, L.; Lei, Z.; Hossain, M. A.; Camarena, S.; Dodson, R. A.; Cook, R. D.; Dutcher, C. S.; Ault, A. P., Direct determination of aerosol pH: size-resolved measurements of submicrometer and supermicrometer aqueous particles. *Anal. Chem.* **2018,** *90*, (19), 11232-11239.
72. Imre, D. G., Xu ,J., Tang, I. N., McGraw, R., Ammonium bisulfate/water equilibrium and metastability phase diagrams. *J. Phys. Chem. A* **1997,** *101*, 4191-4195.
73. Lambe, A. T.; Ahern, A. T.; Williams, L. R.; Slowik, J. G.; Wong, J. P. S.; Abbatt, J. P. D.; Brune, W. H.; Ng, N. L.; Wright, J. P.; Croasdale, D. R.; Worsnop, D. R.; Davidovits, P.; Onasch, T. B., Characterization of aerosol photooxidation flow reactors: heterogeneous oxidation, secondary organic aerosol formation and cloud condensation nuclei activity measurements. *Atmos. Meas. Tech.* **2011,** *4*, (3), 445-461.
74. Bruns, E. A.; El Haddad, I.; Keller, A.; Klein, F.; Kumar, N. K.; Pieber, S. M.; Corbin, J. C.; Slowik, J. G.; Brune, W. H.; Baltensperger, U.; Prévôt, A. S. H., Inter-comparison of laboratory smog chamber and flow reactor systems on organic aerosol yield and composition. *Atmos. Meas. Tech.* **2015,** *8*, (6), 2315-2332.
75. Lambe, A. T.; Chhabra, P. S.; Onasch, T. B.; Brune, W. H.; Hunter, J. F.; Kroll, J. H.; Cummings, M. J.; Brogan, J. F.; Parmar, Y.; Worsnop, D. R.; Kolb, C. E.; Davidovits, P., Effect of oxidant concentration, exposure time, and seed particles on secondary organic aerosol chemical composition and yield. *Atmos. Chem. Phys.* **2015,** *15*, (6), 3063-3075.
76. Pieber, S. M.; Kumar, N. K.; Klein, F.; Comte, P.; Bhattu, D.; Dommen, J.; Bruns, E. A.; Kılıç, D.; El Haddad, I.; Keller, A.; Czerwinski, J.; Heeb, N.; Baltensperger, U.; Slowik, J. G.; Prévôt, A. S. H., Gas-phase composition and secondary organic aerosol formation from standard and particle filter-retrofitted gasoline direct injection vehicles investigated in a batch and flow reactor. *Atmos. Chem. Phys.* **2018,** *18*, (13), 9929-9954.

77. Shrestha, M.; Zhang, Y.; Ebben, C. J.; Martin, S. T.; Geiger, F. M., Vibrational sum frequency generation spectroscopy of secondary organic material produced by condensational growth from alpha-pinene ozonolysis. *J. Phys. Chem. A* **2013,** *117*, (35), 8427-8436.
78. Zanca, N.; Lambe, A. T.; Massoli, P.; Paglione, M.; Croasdale, D. R.; Parmar, Y.; Tagliavini, E.; Gilardoni, S.; Decesari, S., Characterizing source fingerprints and ageing processes in laboratory-generated secondary organic aerosols using proton-nuclear magnetic resonance (1H-NMR) analysis and HPLC HULIS determination. *Atmos. Chem. Phys.* **2017,** *17*, (17), 10405-10421.
79. Lambe, A.; Massoli, P.; Zhang, X.; Canagaratna, M.; Nowak, J.; Daube, C.; Yan, C.; Nie, W.; Onasch, T.; Jayne, J.; Kolb, C.; Davidovits, P.; Worsnop, D.; Brune, W., Controlled nitric oxide production via O(1D) + N2O reactions for use in oxidation flow reactor studies. *Atmos. Meas. Tech.* **2017,** *10*, (6), 2283-2298.
80. Palm, B. B.; Campuzano-Jost, P.; Ortega, A. M.; Day, D. A.; Kaser, L.; Jud, W.; Karl, T.; Hansel, A.; Hunter, J. F.; Cross, E. S.; Kroll, J. H.; Peng, Z.; Brune, W. H.; Jimenez, J. L., In situ secondary organic aerosol formation from ambient pine forest air using an oxidation flow reactor. *Atmos. Chem. Phys.* **2016,** *16*, (5), 2943-2970.
81. Tkacik, D. S.; Lambe, A. T.; Jathar, S.; Li, X.; Presto, A. A.; Zhao, Y.; Blake, D.; Meinardi, S.; Jayne, J. T.; Croteau, P. L.; Robinson, A. L., Secondary organic aerosol formation from in-use motor vehicle emissions using a potential aerosol mass reactor. *Environ Sci Technol* **2014,** *48*, (19), 11235-11242.
82. Bahreini, R., Middlebrook, A. M., Brock, C. A., de Gouw, J. A., McKeen, S. A.,Williams, L. R., Daumit, K. E., Lambe, A. T., Massoli, P., Canagaratna, M. R., Ahmadov, R.,Carrasquillo, A. J., Cross, E. S., Ervens, B., Holloway, J. S.,Hunter, J. F., Onasch, T. B., Pollack, I. B., Roberts, J. M., Ryerson, T. B., Warneke, C., Davidovits, P., Worsnop, D. R., Kroll, J. H., Mass spectral analysis of organic aerosol formed downwind of the Deepwater Horizon oil spill: field studies and laboratory confirmation. *Environ. Sci. Technol.* **2012,** *46*, 8025−8034.
83. Ortega, A. M.; Hayes, P. L.; Peng, Z.; Palm, B. B.; Hu, W.; Day, D. A.; Li, R.; Cubison, M. J.; Brune, W. H.; Graus, M.; Warneke, C.; Gilman, J. B.; Kuster, W. C.; de Gouw, J.; Gutiérrez-Montes, C.; Jimenez, J. L., Real-time measurements of secondary organic aerosol formation and aging from ambient air in an oxidation flow reactor in the Los Angeles area. *Atmos. Chem. Phys.* **2016,** *16*, (11), 7411-7433.
84. Zhang, Z.; Lin, Y. H.; Zhang, H.; Surratt, J. D.; Ball, L. M.; Gold, A., Technical Note: Synthesis of isoprene atmospheric oxidation products: isomeric epoxydiols and the rearrangement products cis- and trans-3-methyl-3,4-dihydroxytetrahydrofuran. *Atmos. Chem. Phys.* **2012,** *12*, (18), 8529-8535.
85. Midgley, P. A.; Weyland, M.; Thomas, J. M.; Johnson, B. F. G., Z-Contrast tomography: a technique in three-dimensional nanostructural analysis based on Rutherford scattering. *Chem. Comm.* **2001**, (10), 907-908.
86. DeCarlo, P. F.; Slowik, J. G.; Worsnop, D. R.; Davidovits, P.; Jimenez, J. L., Particle morphology and density characterization by combined mobility and aerodynamic diameter measurements. part 1: theory. *Aerosol. Sci. Technol.* **2004,** *38*, (12), 1185-1205.
87. Bondy, A. L.; Kirpes, R. M.; Merzel, R. L.; Pratt, K. A.; Banaszak Holl, M. M.; Ault, A. P., Atomic force microscopy-infrared spectroscopy of individual atmospheric aerosol

particles: subdiffraction limit vibrational spectroscopy and morphological analysis. *Anal. Chem.* **2017,** *89*, 8594-8598.

88. DeRieux, W.-S. W.; Li, Y.; Lin, P.; Laskin, J.; Laskin, A.; Bertram, A. K.; Nizkorodov, S. A.; Shiraiwa, M., Predicting the glass transition temperature and viscosity of secondary organic material using molecular composition. *Atmos. Chem. Phys* **2018,** *18*, (9), 6331-6351.
89. Koop, T.; Bookhold, J.; Shiraiwa, M.; Poschl, U., Glass transition and phase state of organic compounds: dependency on molecular properties and implications for secondary organic aerosols in the atmosphere. *Phys. Chem. Chem. Phys.* **2011,** *13*, (43), 19238–19255.
90. Shiraiwa, M., Ammann, M., Koop, T., Pöschl, U., Gas uptake and chemical aging of semisolid organic aerosol particles. *Proc. Natl. Acad. Sci. U. S. A.* **2011,** *103*, (27), 11003–11008.
91. Lee, H. D.; Kaluarachchi, C. P.; Hasenecz, E. S.; Zhu, J. Z.; Popa, E.; Stone, E. A.; Tivanski, A. V., Effect of dry or wet substrate deposition on the organic volume fraction of core–shell aerosol particles. *Atmos. Meas. Tech.* **2019,** *12*, (3), 2033-2042.
92. Liu, P.; Li, Y. J.; Wang, Y.; Bateman, A. P.; Zhang, Y.; Gong, Z.; Bertram, A. K.; Martin, S. T., Highly viscous states affect the browning of atmospheric organic particulate matter. *ACS Cent. Sci.* **2018,** *4*, (2), 207-215.
93. Fard, M. M.; Krieger, U. K.; Peter, T., Kinetic limitation to inorganic ion diffusivity and to coalescence of inorganic inclusions in viscous liquid-liquid phase-separated particles. *J. Phys. Chem. A* **2017,** *121*, 9284-9296.
94. Rindelaub, J. D.; Craig, R. L.; Nandy, L.; Bondy, A. L.; Dutcher, C. S.; Shepson, P. B.; Ault, A. P., Direct measurement of pH in individual particles via Raman microspectroscopy and variation in acidity with relative humidity. *J. Phys. Chem. A* **2016,** *120*, (6), 911-917.
95. Craig, R. L.; Nandy, L.; Axson, J. L.; Dutcher, C. S.; Ault, A. P., Spectroscopic determination of aerosol pH from acid-base equilibria in inorganic, organic, and mixed systems. *J. Phys. Chem. A* **2017,** *121*, (30), 5690-5699.
96. Craig, R. L.; Bondy, A. L.; Ault, A. P., Computer-controlled Raman microspectroscopy (CC-Raman): A method for the rapid characterization of individual atmospheric aerosol particles. *Aerosol. Sci. Technol.* **2017,** *51*, 1099–1112.
97. Ault, A. P.; Zhao, D.; Ebben, C. J.; Tauber, M. J.; Geiger, F. M.; Prather, K. A.; Grassian, V. H., Raman microspectroscopy and vibrational sum frequency generation spectroscopy as probes of the bulk and surface compositions of size-resolved sea spray aerosol particles. *Phys. Chem. Chem. Phys.* **2013,** *15*, (17), 6206-6214.
98. Venkateswarlu, P., Bist, H. D., Jain, Y. S., Laser excited Raman spectrum of ammonium sulfate single crystal. *J. Raman Spectrosc.* **1975,** *3*, 143-151.
99. Jentzsch, P. V.; Kampe, B.; Ciobota, V.; Rosch, P.; Popp, J., Inorganic salts in atmospheric particulate matter: Raman spectroscopy as an analytical tool. *Spectrochim. Acta A Molec. Biomolec. Spectrosc.* **2013,** *115*, 697-708.
100. Sobanska, S.; Hwang, H.; Choel, M.; Jung, H. J.; Eom, H. J.; Kim, H.; Barbillat, J.; Ro, C. U., Investigation of the chemical mixing state of individual Asian dust particles by the combined use of electron probe X-ray microanalysis and Raman microspectrometry. *Anal. Chem.* **2012,** *84*, (7), 3145−3154.
101. Zhou, Q.; Pang, S. F.; Wang, Y.; Ma, J. B.; Zhang, Y. H., Confocal Raman studies of the evolution of the physical state of mixed phthalic acid/ammonium sulfate aerosol droplets and the effect of substrates. *J. Phys. Chem. B* **2014,** *118*, (23), 6198−6205.

102. Riva, M.; Budisulistiorini, S. H.; Chen, Y.; Zhang, Z.; D'Ambro, E. L.; Zhang, X.; Gold, A.; Turpin, B. J.; Thornton, J. A.; Canagaratna, M. R.; Surratt, J. D., Chemical characterization of secondary organic aerosol from oxidation of isoprene hydroxyhydroperoxides. *Envion. Sci. Tech.* **2016,** *50*, (18), 9889-9899.
103. Hatch, L. E.; Creamean, J. M.; Ault, A. P.; Surratt, J. D.; Chan, M. N.; Seinfeld, J. H.; Edgerton, E. S.; Su, Y.; Prather, K. A., Measurements of isoprene-derived organosulfates in ambient aerosols by aerosol time-of-flight mass spectrometry - part 1: single particle atmospheric observations in Atlanta. *Environ. Sci. Technol.* **2011,** *45*, (12), 5105–5111.
104. Hatch, L. E.; Creamean, J. M.; Ault, A. P.; Surratt, J. D.; Chan, M. N.; Seinfeld, J. H.; Edgerton, E. S.; Su, Y.; Prather, K. A., Measurements of isoprene-derived organosulfates in ambient aerosols by aerosol time-of-flight mass spectrometry-part 2: temporal variability and formation mechanisms. *Environ. Sci. Technol.* **2011,** *45*, (20), 8648-8655.
105. Weber, R. J., Guo, H., Russell, A. G., Nenes, A., High aerosol acidity despite declining sulfate concentrations over the past 15 years. *Nat. Geosci. Lett.* **2016,** *9*, 282-286.
106. Riva, M.; Chen, Y.; Zhang, Y.; Lei, Z.; Olson, N.; Boyer, H. C.; Narayan, S.; Yee, L. D.; Green, H.; Cui, T.; Zhang, Z.; Baumann, K. D.; Fort, M.; Edgerton, E. S.; Budisulistiorini, S.; Rose, C. A.; Ribeiro, I.; e Oliveira, R. L.; Santos, E.; Szopa, S.; Machado, C.; Zhao, Y.; Alves, E.; de Sa, S.; Hu, W.; Knipping, E.; Shaw, S.; Duvoisin Junior, S.; Souza, R. A. F. d.; Palm, B. B.; Jimenez, J. L.; Glasius, M.; Goldstein, A. H.; Pye, H. O. T.; Gold, A.; Turpin, B. J.; Vizuete, W.; Martin, S. T.; Thornton, J.; Dutcher, C. S.; Ault, A. P.; Surratt, J. D., Increasing isoprene epoxydiol-to-inorganic sulfate aerosol (IEPOX:Sulfinorg) ratio results in extensive conversion of inorganic sulfate to organosulfur forms: implications for aerosol physicochemical properties. *Environ. Sci. Technol.* **2019,** *Just accepted,* DOI: https://doi.org/10.1021/acs.est.9b01019.
107. Pye, H. O.; Pinder, R. W.; Piletic, I. R.; Xie, Y.; Capps, S. L.; Lin, Y. H.; Surratt, J. D.; Zhang, Z.; Gold, A.; Luecken, D. J.; Hutzell, W. T.; Jaoui, M.; Offenberg, J. H.; Kleindienst, T. E.; Lewandowski, M.; Edney, E. O., Epoxide pathways improve model predictions of isoprene markers and reveal key role of acidity in aerosol formation. *Environ. Sci. Technol.* **2013,** *47*, (19), 11056−11064.
108. Schmedding, R.; Ma, M.; Zhang, Y.; Farrell, S.; Pye, H. O. T.; Chen, Y.; Wang, C.-t.; Rasool, Q. Z.; Budisulistiorini, S. H.; Ault, A. P.; Surratt, J. D.; Vizuete, W., α-Pinene-derived organic coatings on acidic sulfate aerosol impacts secondary organic aerosol formation from isoprene in a box model. *Atmos. Environ.* **2019**, in press, DOI: 10.1016/j.atmosenv.2019.06.005.
109. Silvern, R. F.; Jacob, D. J.; Kim, P. S.; Marais, E. A.; Turner, J. R.; Campuzano-Jost, P.; Jimenez, J. L., Inconsistency of ammonium–sulfate aerosol ratios with thermodynamic models in the eastern US: a possible role of organic aerosol. *Atmos. Chem. Phys.* **2017,** *17*, (8), 5107-5118.

For TOC Only

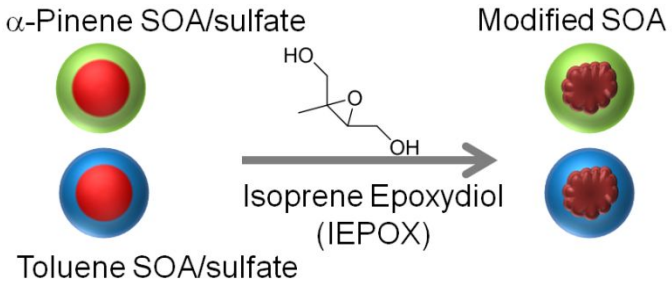
α-Pinene SOA/sulfate
Modified SOA
HO
O
OH
Isoprene Epoxydiol
(IEPOX)
Toluene SOA/sulfate